ACS ORGANIC & INORGANIC Au
AN OPEN ACCESS JOURNAL OF THE AMERICAN CHEMICAL SOCIETY

pubs.acs.org/orginorgau
Article

Unraveling Chlorite Oxidation Pathways in Equatorially Heteroatom-Substituted Nonheme Iron Complexes

Published as part of ACS Organic & Inorganic Auspecial issue"Celebrating the 25th Anniversary of the Chemical Research Society of India".

Limashree Sahoo, Payal Panwar, Chivukula V. Sastri,* and Sam P. de Visser*

Cite This: *ACS Org. Inorg. Au* 2024, 4, 673−680
Read Online
ACCESS | Metrics & More | Article Recommendations | Supporting Information

ABSTRACT: The first-coordination sphere of catalysts is known to play a crucial role in reaction mechanisms, but details of how equatorial ligands influence the reactivity remain unknown. Heteroatom ligated to the equatorial position of iron centers in nonheme iron metalloenzymes modulates structure and reactivity. To investigate the impact of equatorial heteroatom substitution on chlorite oxidation, we synthesized and characterized three novel mononuclear nonheme iron(II) complexes with a pentadentate bispidine scaffold. These complexes feature systematic substitutions at the equatorial position in the bispidine ligand framework where the pyridine group is replaced with NMe_2, SMe, and OMe groups. The three iron(II)−bispidine complexes were subjected to studies in chlorite oxidation reactions as a model pathway for oxygen atom transfer. Chlorine oxyanions, which have the halide in an oxidation state ranging from +1 to +7, have numerous applications but can contaminate water bodies, and this demands urgent environmental remediation. Chlorite, a common precursor to chlorine dioxide, is of particular interest due to the superior antimicrobial activity of chlorine dioxide. Moreover, its generation leads to fewer harmful byproducts in water treatment. Here, we demonstrate that these complexes can produce chlorine dioxide from chlorite in acetate buffer at room temperature and pH 5.0, oxidizing chlorite through the in situ formation of high-valent iron(IV)−oxo intermediates. This study establishes how subtle changes in the coordination sphere around iron can influence the reactivity.

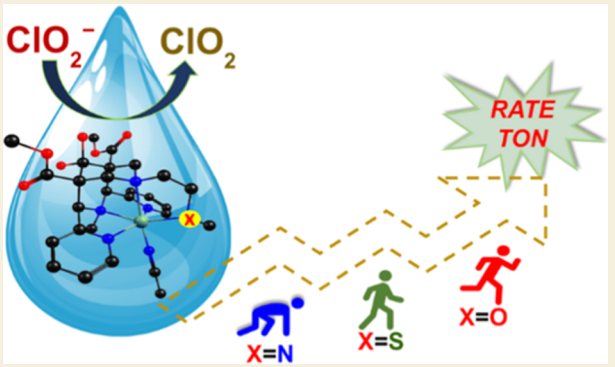

KEYWORDS: *chlorite oxidation, electron transfer, oxygen atom transfer, equatorial perturbation, biomimetic models*

INTRODUCTION

Iron-containing metalloenzymes are well-known for performing essential oxidative transformations in the human body.[1−4] Mononuclear iron enzymes, which are present in nearly all life forms, can be classified into heme and nonheme categories. Heme enzymes include the cytochromes P450 (P450s) and nitric oxide synthases, which feature an axial cysteine unit at the fifth coordination site.[5−10] The nature of this axial ligand is believed to influence the physicochemical properties of compound I (Cpd I). Specifically, the push effect of the thiolate in the Cys axial ligand reduces the electron affinity (or redox potential), thereby increasing the reactivity of Cpd I.[11−15] However, second coordination sphere effects can modulate the push effect of the axial ligand.[16] Nonheme iron dioxygenases, by contrast, show a large variety of ligand coordination types with the cofactor-dependent dioxygenases (tetrahydrobiopterin or α-ketoglutarate) adopting a typical facial coordination with two histidine and one carboxylate amino acid side chain,[17−19] whereas sulfur activating dioxygenases such as cysteine dioxygenase bind the metal through three histidine side chains.[20]

To better understand the functional properties of these metal-containing active sites, biomimetic models have been developed that mimic the coordination environment of the metal and help study the structure, spectroscopy, and reactivity of these complexes.[21−35] Over the past two decades, extensive research has focused on mononuclear nonheme iron complexes with iron(IV)−oxo units supported by polydentate ligands, which resemble intermediates found in metalloenzymes. It has been observed that small changes in the ligand environment may alter reaction pathways and mechanisms.[27−29] Equatorial perturbation in metalloenzymes

Received: June 18, 2024
Revised: August 30, 2024
Accepted: September 5, 2024
Published: September 20, 2024

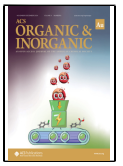

https://doi.org/10.1021/acsorginorgau.4c00045
ACS Org. Inorg. Au 2024, 4, 673−680

refers to modifications in the coordination environment around the metal ion at the enzyme's active site, which can be crucial for its catalytic function. The ligand environment and the first coordination sphere of the iron centers are therefore significant. Researchers have developed biomimetic models with axial and equatorial heteroatom substitutions, achieving changes in reactivity and reaction mechanisms.[34,36−38] Heteroatom substitution can profoundly influence the reactivity of nonheme iron complexes by modifying their electronic properties, ligand field, redox behavior, and ability to engage in secondary interactions. In a computational study, authors have proposed that with the introduction of more sulfur atoms in the equatorial position of iron(IV)−oxo cyclam complexes, the reactivity of C−H activation increases.[39] In this work, we explore the effect of equatorial ligand changes through heteroatom-substituted nonheme iron model complexes on their structure, spectroscopic features, and reactivity patterns. In particular, we investigate chlorite oxidation because this is relevant to the development of environmentally sustainable oxidation processes.

Chlorine oxyanions, with oxidation states ranging from +1 to +7, have a variety of applications, including use as bleaching agents, explosives, herbicides, disinfectants, and oxidants in rocket fuels.[40] Perchlorate, despite its strong oxidizing potential, is quite inert in aqueous solutions, leading to environmental accumulation concerns. Advances have been made in perchlorate remediation using microbes and chemical catalysts.[41−44] Chlorite ions (ClO_2^-) are also utilized as oxidants in diverse areas. Additionally, chlorite ion is a precursor in the generation of chlorine dioxide, which is extensively used in water/wastewater treatment technologies and pulp bleaching.[45−47]

Previous research on catalysts for the one-electron oxidation of chlorite to ClO_2 has predominantly centered on heme-based manganese or iron porphyrin complexes.[48−51] In these catalytic systems, chlorite oxidation is initiated with the oxidation of Mn(II or III) or Fe(III) by chlorite ions, resulting in the formation of high-valent Mn and Fe(IV or V) and hypochlorite ions. Metal ions with elevated oxidation states such as, +IV and +V can directly oxidize chlorite to ClO_2. Lau and co-workers reported on a ruthenium bisphenanthroline complex capable of producing ClO_2.[52] However, there are few reports based on nonheme iron/manganese enzymes for chlorite oxidation. Nam and co-workers demonstrated that under ambient temperature and pH 5.0, two nonheme manganese complexes Mn-BnTPEN and Mn−N4Py [where BnTPEN = *N*-benzyl-*N*,*N*′,*N*′-tris(2-pyridylmethyl)ethane-1,2-diamine and N4Py = *N*,*N*-bis(2-pyridylmethyl)-*N*-bis(2-pyridyl) methylamine] catalyze the formation of chlorine dioxide from chlorite.[53] Additionally, lignin-derived nonheme iron and manganese complexes have been studied for chlorine dioxide production from chlorite in an aqueous solution, employing poly(acrylic acid).[54] Our group has investigated the oxidation of chlorite to chlorine dioxide at ambient temperature and physiological pH using various nonheme iron(II) complexes wherein, we have demonstrated bifurcation of the reaction pathway between electron-transfer vs atom-transfer reactions.[55,56] During these studies, it was reported that changes in the ligand architecture do influence the reaction rates and the mechanistic pathway. In this study, we further explore the influence of equatorial heteroatom substitution on chlorite oxidation. We systematically replaced equatorial pyridine with nitrogen, oxygen, and sulfur in the parent iron bispidine complex (see Figure 1) to investigate how these substitutions influence the overall reaction. This approach will further enhance the general understanding of the ligand environment around the metal center in directing the reaction pathway during chlorite oxidation.

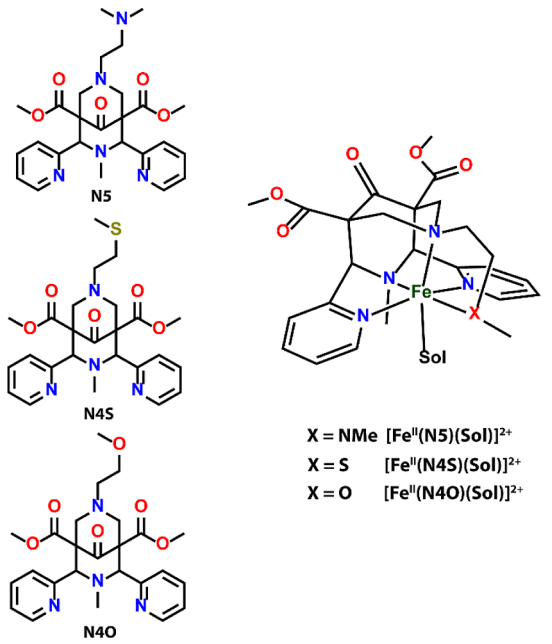

Figure 1. Ligands and the corresponding metal complexes are investigated in this work.

METHODS

Materials

The reactions were conducted by using deionized water, which was obtained through a Millipore Milli-Q water purification system. All chemicals used in the study were obtained from Aldrich Chemical Co. and were of the highest purity available. No further purification was performed. Solvent acetonitrile was dried according to the published procedure and freshly distilled before use.[57] Acetate buffer (pH = 5.0) was used and was freshly prepared for the reactions. The sodium chlorite used as a substrate was obtained from Sigma and underwent purification through recrystallization from an ethanol/water mixture. The piperidone-based ligand N5 was synthesized with a slight modification from a previous report.[58−60] The synthesis of the ligands N4S and N4O was accomplished by replacing *N*,*N*-dimethyl ethylenediamine in the second step of the Mannich reaction with 2-(methylthio)ethylamine and 2-methoxyethylamine, respectively. The metal complexes $[Fe^{II}(N5)](OTf)_2$, $[Fe^{II}(N4S)](OTf)_2$, and $[Fe^{II}(N4O)](OTf)_2$ were synthesized using dry acetonitrile as the solvent inside the glovebox (Jacomex) under an argon gas atmosphere. The detailed experimental procedure is available in the Supporting Information.

Instrumentation

UV−vis spectra and kinetic experiments were recorded on a Hewlett-Packard 8453 spectrophotometer equipped with either a constant temperature circulating water bath or a liquid nitrogen cryostat (Unisoku) with a temperature controller. Nuclear magnetic resonance (NMR) spectra (^1H and $^{13}C\{^1H\}$) were obtained from Bruker AVANCE III HD 400 and 600 MHz NMR spectrometers using tetramethylsilane as the internal standard. High-resolution electrospray ionization mass spectrometry (ESI-MS) spectra were recorded on a Agilent G6546 series ultra-high-performance liquid chromatography (UHPLC)−LC/Q-TOF-high-resolution mass spectrometry mass spectrometer at 298 K with a 2 kV nozzle voltage and 325 °C gas temperature. X-band electron paramagnetic resonance (EPR) was

https://doi.org/10.1021/acsorginorgau.4c00045
ACS Org. Inorg. Au 2024, 4, 673−680

measured on a JES-FA200 ESR spectrometer at 77 K in acetate buffer solution. Experimental conditions (frequency, 9135.99 MHz; power, 0.995 mW; field center, 336.00 mT, width, ±50.00 mT; sweep time, 30.0 s; modulation frequency, 100.00 kHz, width, 2 mT; amplitude CH1 = 10, CH2 = 2.0, and time constant, 0.03 s) were kept the same for all the samples. Electrochemical measurements (cyclic voltammetry (CV) and differential pulse voltammetry were carried out in dry degassed acetonitrile using CH Instruments electrochemical workstation (CHI 1120B) with a glassy carbon working electrode, a Pt-wire auxiliary, and an Ag/AgCl reference electrode; 0.1 M tetrabutylammonium hexafluorophosphate in acetonitrile was used as the electrolyte. All of the values were reported against Ag/Ag^+ and calibrated with the Fc^+/Fc couple. Single-crystal data analysis for the crystals of $[Fe^{II}N4S]^{2+}$ and $[Fe^{II}N4O]^{2+}$ was collected at room temperature using a single source Super Nova CCD System instrument from Agilent Technologies equipped with a fine focus 1.75 kW sealed tube with Mo−Kα radiation. The data were reduced using CrysAlis RED36. The structure solution and refinement were performed using SHELXL97 and Olex2 1.5 programs. CIF check was carried out and submitted to the repository of CCDC.

Reactivity Studies

All of the reactions were run in triplicate in a 10 mm path length quartz cuvette by monitoring the UV−vis spectral changes of the reaction solutions. The formation of the ClO_2 was monitored with the increase in absorbance at its characteristic wavelength at 360 nm in the UV−vis spectrum as a function of time. The rate constants were determined under pseudo-first-order conditions with excess chlorite concentrations (8 mM) with varying concentrations of iron(II) complexes.

o-Tolidine Product Analysis

Chlorate content was determined using 3,3′-dimethyl-4,4′-diaminobiphenyl (*o*-tolidine), as described previously.[55,56] A typical reaction was carried out with 10 μM Fe(II) oxidant, 4.0 mM $NaClO_2$, and 1 mM *o*-tolidine in acetate buffer at ambient temperature. The resulting *o*-tolidine product was extracted from the aqueous medium into ethyl acetate and subsequently analyzed by ESI-MS.

RESULTS AND DISCUSSION

Our initial work started by synthesizing the pentadentate ligand frameworks (namely; N5, N4S, and N4O). N5 was synthesized by using previously reported procedures.[58−60] The ligands N4S and N4O were synthesized following the same protocol as that of N5. Thereafter, the corresponding metal complexes were prepared by dropwise addition of an acetonitrile solution containing $Fe^{II}(OTf)_2{\cdot}2CH_3CN$ to predissolved ligand solution (see the Supporting Information for detailed description). The final complexes were obtained by ether layering of the reaction mixture, resulting in obtaining the desired product. The complex $[Fe^{II}(N5)]^{2+}$ gave yellow colored solid while the complexes $[Fe^{II}(N4O)]^{2+}$ and $[Fe^{II}(N4S)]^{2+}$ yielded yellow and brown colored solids, respectively. The obtained metal complexes were characterized by UV−visible (UV−vis) spectroscopy, ESI-MS, CV, solution state spin only magnetic moment using modified Evans method, and single X-ray crystallography (see Figures S1−S17). The UV−vis spectra of these iron(II) complexes at 298 K show a ligand to metal charge transfer band having a comparable molar extinction coefficient (ε) with a slight shift in λ_{max} values (Table 1). While all three complexes show a signature LMCT band in the region 370−380 nm typical of Fe(II) bispidine complexes,[61] $[Fe^{II}(N4S)]^{2+}$ gives additional shoulder at 428 and 545 nm. These additional spectral features may be due to charge transfer from electron-rich thioether S to iron (Supporting Information Figure S9). The complexes were further characterized using ESI-MS at 298 K. The positive ion

Table 1. Wavelength, Redox Potential, and Kinetics Data (Second-Order Rate Constants, Product Yields, and Turnover Numbers for the Oxidation of ClO_2^- in Aqueous Acetate Buffer) of Iron(II) Complexes

complex	N5	N4S	N4O	L2[55,61]
λ_{max} (nm)[a]	37 (1061)	380 (1057), 428 (573), 545 (60)	373 (1112)	390
$E_{1/2}$ (mV)	1311	1168	1111	n.d.[b]
k_2 (M^{-1} s^{-1})	34	445	514	31
% ClO_2	12	15	18	10
TON	30	233	242	25

[a]Values in parentheses are molar absorbance coefficient (M^{-1} cm^{-1}). [b]n.d. not determined.

scan for $[Fe^{II}(N5)]^{2+}$ complex in acetonitrile gave major signals at m/z = 700.13 which corresponds to $[Fe^{II}(N5)(OTf)]^+$. Another strong signal at m/z = 275.59 was also seen, which could be attributed to $[Fe^{II}(N5)]^{2+}$ species. Additionally, the peak at m/z = 718.14 corresponds to $[Fe^{II}(N5)(OTf)(H_2O)]^+$. For the complex $[Fe^{II}(N4S)]^{2+}$ two significant peaks were observed at m/z = 721.08 and m/z = 286.07 corresponding to $[Fe^{II}(N4S)(OTf)(H_2O)]^+$ and $[Fe^{II}(N4S)]^{2+}$, respectively. The ESI-MS spectrum for the $[Fe^{II}(N4O)]^{2+}$ complex gave two sets of significant signals. The set at m/z = 705.11 and m/z = 687.10 corresponds to $[Fe^{II}(N4O)(OTf)(H_2O)]^+$ and $[Fe^{II}(N4O)(OTf)]^+$, respectively, while the second set at m/z = 278.08 and m/z = 269.07 can be assigned to $[Fe^{II}(N4O)(H_2O)]^{2+}$ and $[Fe^{II}(N4O)]^{2+}$. These assignments are further confirmed by their signature isotopic distribution patterns, as given in the inset of the figures (Supporting Information Figures S10−S13)

To have a better understanding of the nature of the coordination around the iron center, we further carried out CV (polarographic) and differential pulse voltammogram studies of the three complexes. It is interesting to note that $[Fe^{II}(N5)]^{2+}$ shows an irreversible couple with $E_{1/2}$ at 1311 mV against Ag/Ag^+ electrode. On the contrary, the heteroatom substitution of N5 replaced with sulfur or oxygen resulted in irreversible/quasi-irreversible Fe(II)/Fe(III) redox couples. Additionally, it was observed that upon replacing NMe_2 with SMe or OMe has resulted in lowering the Fe(III)/Fe(II) couple by about 143 mV and 200 mV for $[Fe^{II}N4S]^{2+}$ and $[Fe^{II}N4O]^{2+}$, respectively (Table 1 and Supporting Information Figure S14). The irreversible feature of the cyclic voltammogram indicates that these could be high-spin Fe(II) complexes. These results clearly indicate that the replacement of NMe_2 with SMe and OMe has significantly brought the Fe(III)/Fe(II) potential significantly. However, it is worth noting that the difference in the Fe(III)/Fe(II) couple for SMe and OMe ligated Fe(II) complexes differ marginally. This suggests that the nature of the equatorial heteroatom significantly affects the electronic environment of the iron center. To determine the spin state of these iron(II) complexes, the modified ^2H Evans method was employed using CD_3CN and $CDCl_3$ as the markers.[62] The effective magnetic moment was calculated, and the values suggest that these complexes exist in a high-spin S = 2 state (see Supporting Information Figure S15)

The structural characterizations of these new complexes $[Fe^{II}(N4S)]^{2+}$ and $[Fe^{II}(N4O)]^{2+}$ were carried out by single-crystal XRD which clearly shows the penta-*co*-ordination of ligands N4S and N4O, indicating equatorial sulfur and oxygen

https://doi.org/10.1021/acsorginorgau.4c00045
ACS Org. Inorg. Au 2024, 4, 673−680

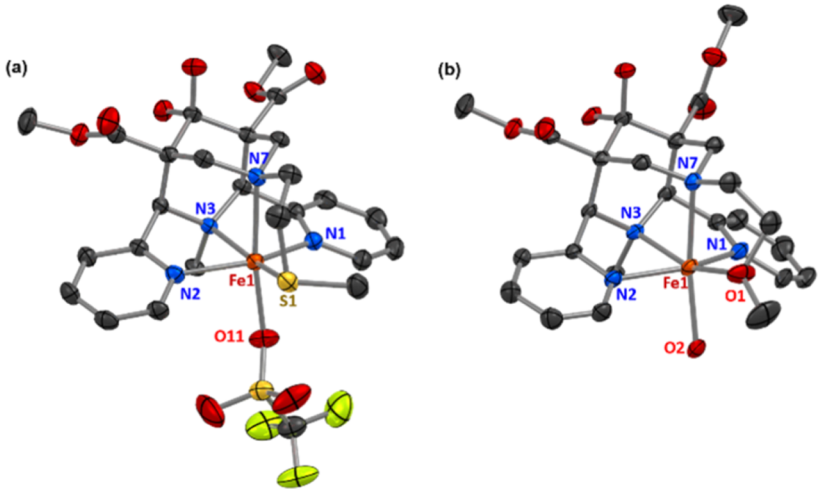

Figure 2. ORTEP diagrams (with 30% ellipsoid probability) of complexes (a) $[Fe^{II}(N4S)]^{2+}$ and (b) $[Fe^{II}(N4O)]^{2+}$. Color coding: carbon (gray), iron (orange), nitrogen (blue) oxygen (red), and sulfur (yellow). Hydrogen atoms and counterions have been omitted for clarity.

ligation to the iron center, respectively (Figure 2a,b). In the sixth coordination position, trans to the N7, the solvent H_2O occupies this position in $[Fe^{II}(N4O)]^{2+}$, while the OTf counteranion occupies it in $[Fe^{II}(N4S)]^{2+}$. The bond angle for ∠N7−Fe1−O_{OTf} is 172° while ∠N7−Fe1−O_{H2O} is 167.45°, and other bond angles suggest that these complexes exist as distorted octahedral geometry. The bond length Fe1−S1(2.510 Å) is somewhat longer than Fe1−O1 (2.116 Å). Furthermore, the average bond length is higher in the case of $[Fe^{II}(N4S)]^{2+}$ compared to that of $[Fe^{II}(N4O)]^{2+}$, which is due to the larger size of sulfur and also the longer bond length of Fe1−S1 (2.510 Å). The Fe1−O_{OTf} ($[Fe^{II}(N4S)]^{2+}$)/Fe1−$O2_{H2O}$ ($[Fe^{II}(N4O)]^{2+}$) and the average bond length of these complexes suggest a high-spin character of the metal.[28,63] Unfortunately we could not crystallize the structure of $[Fe^{II}(N5)]^{2+}$, hence we have optimized its structure using density functional theory to get the information on the bond length and angle (Supporting Information Figure S18 and Table S5). The other bond angles and bond lengths are shown in the Supporting Information in Tables S3 and S4.

With well-characterized Fe(II) complexes on hand, we then studied the oxidation of chlorite (ClO_2^-). Upon the addition of iron(II) complexes (40 μ M) to a solution containing 8 mM sodium chlorite in 50 mM acetate buffer at pH 5.0, at room temperature, we observed an increase in UV absorption at 360 nm corresponding to the formation of chlorine dioxide (ε = 1250 M^{-1} cm^{-1}). Simultaneously, there was a decrease in absorption at 260 nm, indicating the consumption of chlorite (Figure 3a) Similar spectral changes were observed for the reactions involving $[Fe^{II}(N5)]^{2+}$ and $[Fe^{II}(N4S)]^{2+}$ complexes (Supporting Information Figures S19 and S20). We measured the change in absorbance from the UV−vis spectra at 360 nm and plotted it as a function of time, which enabled us to determine the pseudo-first-order rate constant (k_{obs}) for the reaction. Subsequently, these observed rate constants at varying iron(II) concentrations were used to calculate second-order rate constants by plotting k_{obs} as a function of the catalyst concentration. The second-order rate constants (k_2) were found to be 34, 445, and 514 M^{-1} s^{-1} for the reaction of sodium chlorite (ClO_2^-) with $[Fe^{II}(N5)]^{2+}$, $[Fe^{II}(N4S)]^{2+}$, and $[Fe^{II}(N4O)]^{2+}$, respectively (Figure 3b). Also, The observed k_2 for $[Fe^{II}(N5)]^{2+}$ is almost comparable to

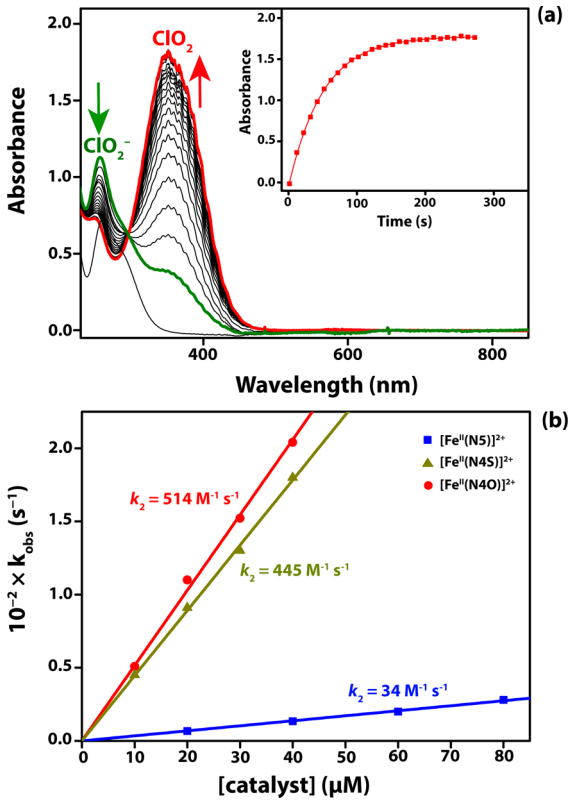

Figure 3. Spectroscopic and kinetic studies of the reaction of iron(II) complexes with ClO_2^-. (a) Upon the addition of 8.0 mM $NaClO_2$ to a solution containing 40 μM $[Fe^{II}(N4O)]^{2+}$ in an acetate buffer, changes in the UV−vis absorption spectra were observed at a scanning interval of 10 s. The inset shows a time trace for the formation of ClO_2. (b) Second-order rate constants were determined for the reaction of ClO_2^- with $[Fe^{II}(N5)]^{2+}$ (blue line), $[Fe^{II}(N4S)]^{2+}$ (yellow line), and $[Fe^{II}(N4O)]^{2+}$ (red line).

the previously reported $[Fe^{II}(L2)]^{2+}$ system, which has nearly a similar ligand structure,[55] and a k_2 of 31 M^{-1} s^{-1}. However, in the heteroatom-substituted (sulfur and oxygen) iron bispidine systems, the reaction rates increase significantly. The reactivity of heteroatom-substituted $[Fe^{II}(N4S)]^{2+}$ and $[Fe^{II}(N4O)]^{2+}$ is nearly 15 times faster than that of their nitrogen analogue, i.e.,

https://doi.org/10.1021/acsorginorgau.4c00045
ACS Org. Inorg. Au 2024, 4, 673−680

$[Fe^{II}(N5)]^{2+}/[Fe^{II}(L2)]^{2+}$.[55] This finding aligns with our recent work, where we observed a nine-fold increase in the rate of sulfoxidation reactions with sulfur-containing systems compared to nitrogen systems. Moreover, we noted a change in the reaction mechanism from oxygen atom transfer to electron transfer in sulfoxidation reactions and from hydrogen atom transfer to hydride transfer in C−H bond activation reactions. In these C−H bond activation reactions, the sulfur-containing system exhibited rates 2−4 times higher than the nitrogen system.[34] These observations clearly indicate that introducing a sulfur heteroatom in the equatorial position of the ligand framework significantly enhances reactivity.[34]

The two heteroatom-substituted bispidine iron complexes exhibit a comparable rate of chlorite oxidation. However, previous studies have shown that oxygen-containing species exhibit faster reactivity than sulfur- and nitrogen-containing species.[37] Furthermore, the amount of ClO_2 formation was found to be dependent on the chlorite concentration as indicated by absorption maxima (Supporting Information Figures S21−S23). We have also determined that the % yield of ClO_2 on the reaction of 8 mM of chlorite and 40 μM of iron(II) complexes were found to be 12, 15, and 18%, respectively. Also, the turnover numbers were calculated by varying concentrations of chlorite at the fixed metal complex concentration. The TON values were in agreement with the observed reaction rates. These observations of the reactivity and yield are in line with previous studies of analogous ruthenium, manganese, and iron catalysts.[52,53,55]

Previous studies have also shown that the reaction between the iron(II) complexes and ClO_2^- proceeds through a high-valent iron(IV)-oxo intermediate.[55,56] However, in the aforementioned iron(II) systems, this intermediate was not observed upon the addition of a stoichiometric amount of ClO_2^-. Instead, the formation of ClO_2 proceeded via in situ generated iron(IV) oxo. Futile attempts were made to generate iron oxo intermediates of these complexes by using different oxidants at room temperature. This in situ generated Fe^{IV}=O intermediate then reacts with another molecule of ClO_2^-, either through electron transfer, yielding ClO_2, or through direct oxygen atom transfer, predominantly forming ClO_3^- products. These two reaction pathways are energetically comparable.[55] Consequently, the overall reaction requires the involvement of two molecules of chlorite per iron center to produce one molecule of ClO_3^- (or ClO_2).

$$[Fe^{II}]^{2+} + ClO_2^- \rightarrow [Fe^{IV}(O)]^{2+} + ClO^-$$

$$[Fe^{IV}(O)]^{2+} + ClO_2^- \rightarrow [Fe^{III}(O)]^{+} + ClO_2$$

$$[Fe^{IV}(O)]^{2+} + ClO_2^- \rightarrow [Fe^{II}]^{2+} + ClO_3^-$$

To elucidate the mechanism of chlorite oxidation, we employed *o*-tolidine as a model substrate, known to selectively react with ClO_3^-.[55,56,64] When the iron(II) complexes were reacted with 4 mM $NaClO_2$ and 40 μM *o*-tolidine in an acetate buffer at room temperature, we observed a new absorption band at 442 nm (Figure 4a). This band decayed over time, with a new band forming at 388 nm. It is well understood that the formation of 442 nm band in the UV−vis spectra corresponds to the formation of 3,3′-dimethyl-4-amino-4′-nitrobiphenyl ($tolidine^{oxd}$) which proceeds via the formation of 3,3′-dimethyl-4-amino-4′-nitrosobiphenyl (Scheme 1). The 388 nm absorption band is attributed to the formation of ferric-$tolidine^{oxd}$.[55,56,64] It is generally believed that 442 nm band corresponds to the reaction proceeding via atom-transfer reaction, resulting in the oxidation of one of the $-NH_2$ group in *o*-tolidine to −NO and subsequently to $-NO_2$ and the in situ generation Fe^{IV}=O undergoing two electron reduction to Fe^{II}. On the contrary during the electron-transfer reaction in the oxidation of *o*-tolidine Fe^{IV}=O undergoes one electron reduction to Fe^{III}=O which subsequently leads to the formation of ferric complex with a signature peak at 388 nm in the UV−vis spectrum.[55,56,64] In the current study, it was observed that upon addition of the iron(II) complexes results

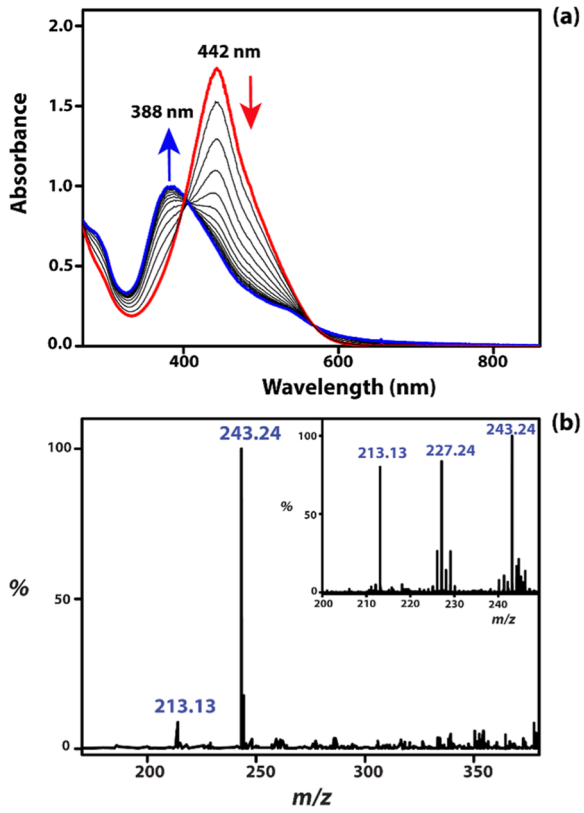

Figure 4. (a) UV−vis absorption spectra of $[Fe^{II}(N4O)]^{2+}$ (10 μM) was recorded after the reaction with 4.0 mM $NaClO_2$ and *o*-tolidine (40 μM) in pH 5 acetate buffer. (b) ESI-MS spectra of the products obtained after the completion of the reaction (4 mM $NaClO_2$ and 1 mM of *o*-tolidine) with $[Fe^{II}(N4O)]^{2+}$ (10 μM), and the inset shows the mass of various oxidation products of *o*-tolidine (sample taken at 60 s) (product + H^+).

Scheme 1. Reaction of *o*-Tolidine with ClO_2^- in the Presence of Iron(II) Complexes

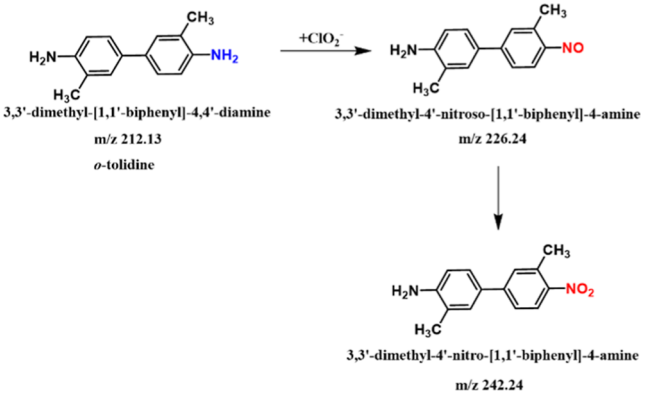

https://doi.org/10.1021/acsorginorgau.4c00045
ACS Org. Inorg. Au 2024, 4, 673−680

in the immediate formation of the 442 nm band. However, the decay of this 442 nm band varied among the complexes: $[Fe^{II}(N5)]^{2+}$ showed the slowest decay, followed by $[Fe^{II}(N4S)]^{2+}$, and $[Fe^{II}(N4O)]^{2+}$ exhibited the fastest decay (Supporting Information Figure S24). The oxidation of *o*-tolidine proceeds by in situ generated Fe^{IV}=O intermediate, resulting in the predominant formation of ClO_3^- through an oxygen atom transfer pathway. This chlorate then reacts with *o*-tolidine, resulting in partially oxidized 3,3′-dimethyl-4-amino-4′-nitrosobiphenyl and eventually, the fully oxidized 3,3′-dimethyl-4-amino-4′-nitrobiphenyl species as observed with the formation of 442 nm absorption band (Figure 4a). However, to understand the formation of the ferric species, further experiments were warranted. To have a clear understanding of the reaction pathway, additional EPR experiments were carried out. The samples were collected immediately upon the formation of 442 nm species (almost instantly) and again after the complete formation of 388 nm species.

The X-band EPR spectra at 77 K of the frozen glass of the reaction mixture immediately after the addition of Fe(II) complexes to the buffer solution containing chlorite and *o*-tolidine can be considered as EPR silent with a trace impurity of Fe(III) species (red line). As the reaction proceeds, resulting in the formation of a 388 nm band, a rhombic signal with $g_x = 2.03$, $g_y = 1.99$, and $g_z = 2.09$ was observed, indicating the formation of a low-spin Fe(III) species (black line) (see Supporting Information Figure S25). Comparing the redox potential values of the complexes and the rate of formation of ferric species from the UV−vis spectrum, it would well be concluded that after the initial atom-transfer reactions, the Fe(II) species generated gets subsequently oxidized to the corresponding Fe(III) complexes. The product analysis of the oxidized *o*-tolidine was carried out by extracting the reaction mixture in ethyl acetate. The ESI-MS spectrum revealed signals at *m*/*z* 213.13, 227.24, and 243.24, corresponding to the starting material *o*-tolidine, the partially oxidized product, and the fully oxidized product, respectively (Figure 4b) (Scheme1). These findings suggest that all of these iron(II) complexes react with chlorite primarily through oxygen atom transfer, leading to the formation of ClO_3^-, followed by oxidation of Fe(II) to form Fe(III).

Previous studies on chlorite oxidation demonstrated that any equatorial perturbation of the systems, such as by methyl substitution in the $[Fe^{II}(O)(N4Py)]^{2+}$ system, shifts the mechanism from electron transfer to oxygen atom transfer. Building on these insights, our current findings indicate that substituting heteroatoms, such as oxygen and sulfur, in place of nitrogen within the ligand framework preserves the oxygen atom transfer mechanism. Moreover, these substitutions significantly enhance the reactivity, yield, and turnover number of the reaction. This suggests that the presence of oxygen and sulfur in the equatorial plane not only supports but also improves the catalytic efficiency of these iron(II) complexes in chlorite oxidation.

CONCLUSIONS

In this study, we have demonstrated the experimental investigations of three nonheme iron(II) complexes, $[Fe^{II}(N5)]^{2+}$, $[Fe^{II}(N4S)]^{2+}$, and $[Fe^{II}(N4O)]^{2+}$, for their ability to oxidize ClO_2^- to ClO_2 at ambient temperature and pH 5.0 in acetate buffer. The work focused on the equatorial perturbation by heteroatom substitution of the systems on the product distribution. The results show that these three complexes react with ClO_2^- via the formation of Fe^{IV}=O intermediate. The rate and yield of ClO_2 and TON were calculated, and the mechanism was established by using *o*-tolidine as the model substrate. Our findings present that all these complexes react with chlorite via an oxygen atom transfer via in situ formation of iron(IV)−oxo species.

ASSOCIATED CONTENT

Data Availability Statement

The data underlying this study are available in this article and its Supporting Information.

Supporting Information

The Supporting Information is available free of charge at https://pubs.acs.org/doi/10.1021/acsorginorgau.4c00045.

Detailed experimental procedures with synthetic approaches of the ligands and their corresponding metal complexes, associated characterization spectral information of the various species, kinetics, Cartesian coordinates, and energy profile of $[Fe(N5)]^{2+}$ (PDF)

Accession Codes

CCDC deposition numbers 2358889 for $[Fe^{II}(N4S)]^{2+}$ and 2358890 for $[Fe^{II}(N4O)]^{2+}$ contain the supplementary crystallographic data for this paper. These data are provided free of charge by The Cambridge Crystallographic Data Centre.

AUTHOR INFORMATION

Corresponding Authors

Chivukula V. Sastri − *Department of Chemistry, Indian Institute of Technology Guwahati, Assam 781039, India;* orcid.org/0000-0003-0477-7741; Email: sastricv@iitg.ac.in

Sam P. de Visser − *Department of Chemistry, Indian Institute of Technology Guwahati, Assam 781039, India; The Manchester Institute of Biotechnology and Department of Chemical Engineering, The University of Manchester, Manchester M1 7DN, U.K.;* orcid.org/0000-0002-2620-8788; Email: sam.devisser@manchester.ac.uk

Authors

Limashree Sahoo − *Department of Chemistry, Indian Institute of Technology Guwahati, Assam 781039, India*

Payal Panwar − *Department of Chemistry, Indian Institute of Technology Guwahati, Assam 781039, India*

Complete contact information is available at: https://pubs.acs.org/10.1021/acsorginorgau.4c00045

Author Contributions

The manuscript was written through the contributions of all authors. All authors have approved the final version of the manuscript.

Notes

The authors declare no competing financial interest.

ACKNOWLEDGMENTS

Research support was provided to C.V.S. by the Department of Science and Technology (SERB), India through the grant code CRG/2023/000456. C.V.S. also acknowledges funding through the Scheme for Transformational and Advanced

Research in Sciences MoE/STARS/2023-0374. We would also like to thank Central Instrument Facility, IIT Guwahati for the Instrumental support. L.S. and P.P. would like to thank MHRD for the fellowship and the Chemistry department for XRD.

ABBREVIATIONS

TON, turnover number; XRD, X-ray diffraction

REFERENCES

(1) Atkins, P. W.; Jones, L. *Chemical Principles*; W. H. Freeman and Co.: New York, 2010.
(2) Kraut, D. A.; Carroll, K. S.; Herschlag, D. Challenges in Enzyme Mechanism and Energetics. *Annu. Rev. Biochem.* **2003**, *72*, 517−571.
(3) Moran, L. A.; Horton, R. A.; Scrimgeour, G.; Perry, M. *Principles of Biochemistry*, 5th ed.; Pearson: Boston, 2012.
(4) Dunham, N. P.; Arnold, F. H. Nature's Machinery, Repurposed: Expanding the Repertoire of Iron-Dependent Oxygenases. *ACS Catal.* **2020**, *10*, 12239−12255.
(5) Meunier, B.; de Visser, S. P.; Shaik, S. Mechanism of Oxidation Reactions Catalyzed by Cytochrome P450 Enzymes. *Chem. Rev.* **2004**, *104*, 3947−3980.
(6) Denisov, I. G.; Makris, T. M.; Sligar, S. G.; Schlichting, I. Structure and Chemistry of Cytochrome P450. *Chem. Rev.* **2005**, *105*, 2253−2278.
(7) *Cytochrome P450: Structure, Mechanism and Biochemistry*, 3rd ed.; de Montellano, O., Ed.; Kluwer Academic/Plenum Publishers: New York, 2005.
(8) Stuehr, D. J. Mammalian nitric oxide synthases. *Biochim. Biophys. Acta, Bioenerg.* **1999**, *1411*, 217−230.
(9) Poulos, T. L.; Follmer, A. H. Updating the paradigm: redox partner binding and conformational dynamics in cytochromes P450. *Acc. Chem. Res.* **2022**, *55*, 373−380.
(10) Wei, C.-C.; Crane, B. R.; Stuehr, D. J. Tetrahydrobiopterin-radical enzymology. *Chem. Rev.* **2003**, *103*, 2365−2384.
(11) Dawson, J. H.; Holm, R. H.; Trudell, J. R.; Barth, G.; Linder, R. E.; Bunnenberg, E.; Djerassi, C.; Tang, S. C. Magnetic circular dichroism studies. 43. Oxidized cytochrome P-450. Magnetic circular dichroism evidence for thiolate ligation in the substrate-bound form. Implications for the catalytic mechanism. *J. Am. Chem. Soc.* **1976**, *98*, 3707−3709.
(12) Poulos, T. L. The role of the proximal ligand in heme enzymes. *J. Biol. Inorg. Chem.* **1996**, *1*, 356−359.
(13) Ogliaro, F.; de Visser, S. P.; Shaik, S. The "push" effect of the thiolate ligand in cytochrome P450: a theoretical gauging. *J. Inorg. Biochem.* **2002**, *91*, 554−567.
(14) Stone, K. L.; Behan, R. K.; Green, M. T. Resonance Raman spectroscopy of chloroperoxidase compound II provides direct evidence for the existence of an iron (IV)−hydroxide. *Proc. Natl. Acad. Sci. U.S.A.* **2006**, *103*, 12307−12310.
(15) McQuarters, A. B.; Speelman, A. L.; Chen, L.; Elmore, B. O.; Fan, W.; Feng, C.; Lehnert, N. Exploring second coordination sphere effects in nitric oxide synthase. *J. Biol. Inorg. Chem.* **2016**, *21*, 997−1008.
(16) Amanullah, S. K.; Singha, A.; Dey, A. Tailor made iron porphyrins for investigating axial ligand and distal environment contributions to electronic structure and reactivity. *Coord. Chem. Rev.* **2019**, *386*, 183−208.
(17) Roberts, K. M.; Fitzpatrick, P. F. Mechanisms of tryptophan and tyrosine hydroxylase. *IUBMB Life* **2013**, *65*, 350−357.
(18) Costas, M.; Mehn, M. P.; Jensen, M. P.; Que, L., Jr. Dioxygen activation at mononuclear non-heme iron active sites: Enzymes, models, and intermediates. *Chem. Rev.* **2004**, *104*, 939−986.
(19) *Iron-Containing Enzymes: Versatile Catalysts of Hydroxylation Reactions in Nature*; de Visser, S. P., Kumar, D., Eds.; Royal Society of Chemistry Publishing: Cambridge (UK), 2011; .
(20) de Visser, S. P. Elucidating enzyme mechanism and intrinsic chemical properties of short-lived intermediates in the catalytic cycles of cysteine dioxygenase and taurine/a-ketoglutarate dioxygenase. *Coord. Chem. Rev.* **2009**, *253*, 754−768.
(21) Buongiorno, D.; Straganz, G. D. Structure and function of atypically coordinated enzymatic mononuclear non-heme-Fe(II) centers. *Coord. Chem. Rev.* **2013**, *257*, 541−563.
(22) Atanasov, M.; Comba, P.; Hausberg, S.; Martin, B. Cyanometalate-Bridged Oligonuclear Transition Metal Complexes-Possibilities for a Rational Design of SMMs. *Coord. Chem. Rev.* **2009**, *253*, 2306−2314.
(23) Sorokin, A. B. Phthalocyanine Metal Complexes in Catalysis. *Chem. Rev.* **2013**, *113*, 8152−8191.
(24) Ray, K.; Pfaff, F. F.; Wang, B.; Nam, W. Status of Reactive Non-Heme Metal-Oxygen Intermediates in Chemical and Enzymatic Reactions. *J. Am. Chem. Soc.* **2014**, *136*, 13942−13958.
(25) Oloo, W. N.; Que, L., Jr. Bioinspired Nonheme Iron Catalysts for C−H and C=C Bond Oxidation: Insights into the Nature of the Metal-Based Oxidants. *Acc. Chem. Res.* **2015**, *48*, 2612−2621.
(26) Nam, W.; Lee, Y.-M.; Fukuzumi, S. Hydrogen Atom Transfer Reactions of Mononuclear Non-heme Metal−Oxygen Intermediates. *Acc. Chem. Res.* **2018**, *51*, 2014−2022.
(27) Mukherjee, G.; Lee, C. W. Z.; Nag, S. S.; Alili, A.; Cantú Reinhard, F. G.; Kumar, D.; Sastri, C. V.; de Visser, S. P. Dramatic rate-enhancement of oxygen atom transfer by an iron(IV) oxo species by equatorial ligand field perturbations. *Dalton Trans.* **2018**, *47*, 14945−14957.
(28) Mukherjee, G.; Alili, A.; Barman, P.; Kumar, D.; Sastri, C. V.; de Visser, S. P. Interplay between steric and electronic effects: A joint spectroscopy and computational study of non-heme iron(IV)-oxo complexes. *Chem.—Eur. J.* **2019**, *25*, 5086−5098.
(29) Mukherjee, G.; Satpathy, J. K.; Bagha, U. K.; Mubarak, M. Q. E.; Sastri, C. V.; de Visser, S. P. Inspiration from Nature: influence of engineered ligand scaffolds and auxiliary factors on the reactivity of biomimetic oxidants. *ACS Catal.* **2021**, *11*, 9761−9797.
(30) de Visser, S. P.; Lin, Y.-T.; Ali, H. S.; Bagha, U. K.; Mukherjee, G.; Sastri, C. V. Negative catalysis/non-Bell-Evans-Polanyi reactivity by metalloenzymes: Examples from mononuclear heme and non-heme iron oxygenases. *Coord. Chem. Rev.* **2021**, *439*, 213914.
(31) McDonald, A. R.; Que, L., Jr. High-valent non-heme iron-oxo complexes: Synthesis, structure, and spectroscopy. *Coord. Chem. Rev.* **2013**, *257*, 414−428.
(32) Rasheed, W.; Draksharapu, A.; Banerjee, S.; Young, V. G., Jr.; Fan, R.; Guo, Y.; Ozerov, M.; Nehrkorn, J.; Krzystek, J.; Telser, J.; Que, L., Jr Crystallographic Evidence for a Sterically Induced Ferryl Tilt in a Non-Heme Oxoiron (IV) Complex that Makes it a Better Oxidant. *Angew. Chem.* **2018**, *130*, 9531−9535.
(33) Nam, W.; Lee, Y.-M.; Fukuzumi, S. Tuning reactivity and mechanism in oxidation reactions by mononuclear non-heme iron(IV)-oxo complexes. *Acc. Chem. Res.* **2014**, *47*, 1146−1154.
(34) Satpathy, J. K.; Yadav, R.; Bagha, U. K.; Kumar, D.; Sastri, C. V.; de Visser, S. P. Enhanced Reactivity through Equatorial Sulfur Coordination in Non-heme Iron(IV)−Oxo Complexes: Insights from Experiment and Theory. *Inorg. Chem.* **2024**, *63*, 6752−6766.
(35) Mitra, M.; Nimir, H.; Demeshko, S.; Bhat, S. S.; Malinkin, S. O.; Haukka, M.; Fillol, L.; Lisensky, G. C.; Meyer, F.; Shteinman, A. A.; Browne, W. R.; Hrovat, D. A.; Richmond, M. G.; Costas, M.; Nordlander, E. Non-heme Fe(IV) Oxo Complexes of Two New Pentadentate Ligands and Their Hydrogen-Atom and Oxygen-Atom Transfer Reactions. *Inorg. Chem.* **2015**, *54*, 7152−7164.
(36) Deutscher, J.; Gerschel, P.; Warm, K.; Kuhlmann, U.; Mebs, S.; Haumann, M.; Dau, H.; Hildebrandt, P.; Apfel, U. P.; Ray, K. A bioinspired oxoiron (iv) motif supported on a N2S2 macrocyclic ligand. *Chem. Commun.* **2021**, *57*, 2947−2950.
(37) Monte Pérez, I.; Engelmann, X.; Lee, Y.-M.; Yoo, M.; Kumaran, E.; Farquhar, E. R.; Bill, E.; England, J.; Nam, W.; Swart, M.; Ray, K. A Highly Reactive Oxoiron(IV) Complex Supported by a Bioinspired N3O Macrocyclic Ligand. *Angew. Chem., Int. Ed.* **2017**, *56*, 14384−14388.
(38) Villar-Acevedo, G.; Lugo-Mas, P.; Blakely, M. N.; Rees, J. A.; Ganas, A. S.; Hanada, E. M.; Kaminsky, W.; Kovacs, J. A.

https://doi.org/10.1021/acsorginorgau.4c00045
ACS Org. Inorg. Au 2024, 4, 673−680

Metalassisted oxo atom addition to an Fe (III) thiolate. *J. Am. Chem. Soc.* **2017**, *139*, 119−129.
(39) Kaur, L.; Mandal, D. Role of "S" Substitution on C−H Activation Reactivity of Iron (IV)−Oxo Cyclam Complexes: a Computational Investigation. *Inorg. Chem.* **2022**, *61*, 14582−14590.
(40) Urbansky, E. T.; Schock, M. R. J. Quantitation of Perchlorate Ion: Practices and Advances Applied to the Analysis of Common Matrices. *J. Environ. Manag.* **1999**, *56*, 79−95.
(41) *Perchlorate, Environmental Occurrence, Interactions and Treatment*; Gu, B., Coates, J. D., Eds.; Springer: New York, 2006; p 411.
(42) Coates, J. D.; Achenbach, L. A. *Perchlorate, Environmental Occurrence, Interactions and Treatment*; Gu, B., Coates, J. D., Eds.; Springer: New York, 2006; pp 279−291.
(43) Abu-Omar, M. M. Swift oxo transfer reactions of perchlorate and other substrates catalyzed by rhenium oxazoline and thiazoline complexesElectronic supplementary information (ESI) available: colour versions of Figs. 3 and 4. See http://www.rsc.org/suppdata/cc/b3/b300189j/. *Chem. Commun.* **2003**, 2102−2111.
(44) Hurley, k.D.; Zhang, Y.; Shapley, J. R. Ligand-Enhanced Reduction of Perchlorate in Water with Heterogeneous Re−Pd/C Catalysts. *J. Am. Chem. Soc.* **2009**, *131*, 14172−14173.
(45) Conrad, C. L.; Yin, Y. B.; Hanna, T.; Atkinson, A. J.; Alvarez, P. J.; Tekavec, T. N.; Reynolds, M. A.; Wong, M. S. Fit-for-purpose treatment goals for produced waters in shale oil and gas fields. *Water Res.* **2020**, *173*, 115467.
(46) Erkenbrecher, C. W.; Nurnberg, S.; Breyla, A. D. A Comparison of Three Nonoxidizing Biocides and Chlorine Dioxide in Treating Marcellus Shale Production Waters. *SPE Prod. Oper.* **2015**, *30* (04), 368−374.
(47) Odeh, I. N.; Francisco, J. S.; Margerum, D. W. New pathways for chlorine dioxide decomposition in basic solution. *Inorg. Chem.* **2002**, *41* (24), 6500−6506.
(48) Umile, T. P.; Groves, J. T. Catalytic generation of chlorine dioxide from chlorite using a water-soluble manganese porphyrin. *Angew. Chem., Int. Ed.* **2011**, *50* (3), 695−698.
(49) Umile, T. P.; Wang, D.; Groves, J. T. Dissection of the mechanism of manganese porphyrin-catalyzed chlorine dioxide generation. *Inorg. Chem.* **2011**, *50* (20), 10353−10362.
(50) Hicks, S. D.; Petersen, J. L.; Bougher, C. J.; Abu-Omar, M. M. Chlorite dismutation to chlorine dioxide catalyzed by a water-soluble manganese porphyrin. *Angew. Chem., Int. Ed.* **2011**, *50* (3), 699−702.
(51) Zdilla, M. J.; Lee, A. Q.; Abu-Omar, M. M. Bioinspired dismutation of chlorite to dioxygen and chloride catalyzed by a watersoluble iron porphyrin. *Angew. Chem., Int. Ed.* **2008**, *47* (40), 7697−7700.
(52) Hu, Z.; Du, H.; Man, W.-L.; Leung, C.-F.; Liang, H.; Lau, T.-C. Catalytic reactions of chlorite with a polypyridyl ruthenium(II) complex: disproportionation, chlorine dioxide formation and alcohol oxidation. *Chem. Commun.* **2012**, *48*, 1102−1104.
(53) Hicks, S. D.; Kim, D.; Xiong, S.; Medvedev, G. A.; Caruthers, J.; Hong, S.; Nam, W.; Abu-Omar, M. M. Non-Heme Manganese Catalysts for On-Demand Production of Chlorine Dioxide in Water and Under Mild Conditions. *J. Am. Chem. Soc.* **2014**, *136*, 3680−3686.
(54) Champ, T. B.; Jang, J. H.; Lee, J. L.; Wu, G.; Reynolds, M. A.; Abu-Omar, M. M. Lignin-Derived Non-Heme Iron and Manganese Complexes: Catalysts for the On-Demand Production of Chlorine Dioxide in Water under Mild Conditions. *Inorg. Chem.* **2021**, *60*, 2905−2913.
(55) Barman, P.; Faponle, A. S.; Vardhaman, A. K.; Angelone, D.; Löhr, A. M.; Browne, W. R.; Comba, P.; Sastri, C. V.; de Visser, S. P. Influence of Ligand Architecture in Tuning Reaction Bifurcation Pathways for Chlorite Oxidation by Non-Heme Iron Complexes. *Inorg. Chem.* **2016**, *55*, 10170−10181.
(56) Sahoo, L.; Satpathy, J. K.; Yadav, R.; de Visser, S. P.; Sastri, C. V. Equatorial Perturbation Driven Reaction Bifurcation in Non-Heme Iron Complexes for Chlorite Oxidation. *Eur. J. Inorg. Chem.* **2023**, *26*, No. e202300380.
(57) *Purification of Laboratory Chemicals*; Perrin, D. D., Ed.; Pergamon Press: Oxford, 1997.
(58) Mukherjee, G.; Velmurugan, G.; Kerscher, M.; Kumar Satpathy, J.; Sastri, C. V.; Comba, P. Mechanistic Insights into Amphoteric Reactivity of an Iron-Bispidine Complex. *Chem.—Eur. J.* **2024**, *30*, No. e202303127.
(59) Börzel, H.; Comba, P.; Hagen, K. S.; Lampeka, Y. D.; Lienke, A.; Linti, G.; Merz, M.; Pritzkow, H.; Tsymbal, L. V. Iron Coordination Chemistry with Tetra-Penta- and Hexadentate Bispidine-Type Ligands. *Inorg. Chim. Acta* **2002**, *337*, 407−419.
(60) Barnes, N. A.; Brooker, A. T.; Godfrey, S. M.; Mallender, P. R.; Pritchard, R. G.; Sadler, M. The Synthesis and Structural Characterisation of a Series of Hydrophobic Piperidones and Bispidones. *Eur. J. Org Chem.* **2008**, *2008*, 1019−1030.
(61) Bleher, K.; Comba, P.; Kass, D.; Ray, K.; Wadepohl, H. Reactivities of iron(IV)-oxido compounds with pentadentate bispidine ligands. *J. Inorg. Biochem.* **2023**, *241*, 112123.
(62) Evans, D. F.; Jakubovic, D. A. Water-soluble Hexadentate Schiff-base Ligands as Sequestrating Agents for Iron(III) and Gallium(III). *J. Chem. Soc., Dalton Trans.* **1988**, 2927.
(63) Plaza-Lozano, D.; Ramírez-Palma, D.; Vela, A.; Olguín, J. High spin iron(II) complexes based on imidazolyland 1,2,3-triazolyl-thione ligands and NCE (E = S, Se or BH3) co-ligands: effect of the S-functional group on the structural and magnetic properties. *New J. Chem.* **2022**, *46*, 14910−14921.
(64) Urone, P.; Bonde, E. Colorimetric Determination of Chlorates in Well Waters. *Anal. Chem.* **1960**, *32*, 1666−1668.

https://doi.org/10.1021/acsorginorgau.4c00045
ACS Org. Inorg. Au 2024, 4, 673−680